Nuclear Science and Techniques (2025) 36:194
https://doi.org/10.1007/s41365-025-01779-0

Predictions of complete fusion cross-sections of ^{6,7}Li, ^{9}Be, and ^{10}B using a Bayesian neural network method

Kai-Xuan Cheng[1] · Rong-Xing He[1] · Chun-Yuan Qiao[1] · Chun-Wang Ma[2]

Received: 20 January 2025 / Revised: 6 March 2025 / Accepted: 31 March 2025 / Published online: 31 July 2025

Abstract
A machine learning approach based on Bayesian neural networks was developed to predict the complete fusion cross-sections of weakly bound nuclei. This method was trained and validated using 475 experimental data points from 39 reaction systems induced by ^{6,7}Li, ^{9}Be, and ^{10}B. The constructed Bayesian neural network demonstrated a high degree of accuracy in evaluating complete fusion cross-sections. By comparing the predicted cross-sections with those obtained from a single-barrier penetration model, the suppression effect of ^{6,7}Li and ^{9}Be with a stable nucleus was systematically analyzed. In the cases of ^{6}Li and ^{7}Li, less suppression was predicted for relatively light-mass targets than for heavy-mass targets, and a notably distinct dependence relationship was identified, suggesting that the predominant breakup mechanisms might change in different mass target regions. In addition, minimum suppression factors were predicted to occur near target nuclei with neutron-closed shell.

Keywords Fusion reaction · Weakly bound nuclei · Machine learning · Bayesian neural network

1 Introduction

Advancements in beam quality and detection technology in the latest generation of radiation nuclear beam facilities have brought the study of reaction mechanisms induced by weakly bound nuclei in the Coulomb barrier energy region to the forefront of nuclear physics research [1, 2]. In contrast with the fusion processes involving strongly bound nuclei, the mechanisms triggered by weakly bound nuclei are complex because of their lower binding energies. This complexity is mainly exemplified by the extended nuclear matter distribution and breakup effect [3, 4]. The former, a static effect, results in a reduction in the average fusion barrier height, consequently enhancing the fusion cross-sections. The dynamic breakup of the projectile can diminish the flux of direct fusion reactions, leading to three distinct processes: (1) sequential complete fusion (SCF), where all fragments resulting from the breakup fuse with the target; (2) incomplete fusion (ICF), where only some of the breakup fragments are absorbed by the target; and (3) no capture breakup (NCBU), where none of the breakup fragments are captured by the target. The reaction process, in which the entire projectile without breakup is captured by the target, is termed direct complete fusion (DCF). However, from an experimental perspective, differentiating between the fusion yields of SCF and DCF is challenging. As a result, only complete fusion (CF) cross-sections, including both DCF and SCF cross-sections, can be measured.

Over the past few decades, numerous experimental [5–8] and theoretical [9–11] studies have been conducted on fusion reactions involving weakly bound nuclei. The main objective of these studies was to investigate the influence of breakup on fusion reactions near the Coulomb barrier [12–14]. One of the most widely adopted approaches is to compare data with predictions from a single-barrier penetration model [15, 16] or a coupled channel model without breakup channels [17–19]. It has been demonstrated that the CF cross-sections

This work was supported by National Natural Science Foundation of China (Nos. 12105080 and 12375123), China Postdoctoral Science Foundation (No. 2023M731015), and Natural Science Foundation of Henan Province (No. 242300422048).

✉ Kai-Xuan Cheng
chengkaixuan@htu.edu.cn

✉ Chun-Wang Ma
machunwang@126.com

[1] School of Physics, Centre for Theoretical Physics, Henan Normal University, Xinxiang 453007, China

[2] Institute of Nuclear Science and Technology, Henan Academy of Sciences, Zhengzhou 450015, China

are suppressed at energies near and above the Coulomb barrier [20, 21]. Thus far, the dependence of the suppression effect on the breakup threshold energy of the projectile has been revealed, and an empirical relationship between the suppression factors and threshold energies has been reported [22]. However, suppression phenomena with various target nuclei remain unexplained [14, 23], and no systematic behavior of the CF suppression factors has been observed in the relatively heavy-mass target region [1]. For light- and medium-mass targets, the behavior of the suppression factor has not been fully established because of the experimental difficulty in distinguishing residues from ICF and CF. Therefore, we extended a machine learning method to fusion reactions induced by weakly bound projectiles and analyzed the systematic behavior of suppression factors across various mass target regions.

Bayesian neural networks (BNNs), one of the commonly used machine learning methods, have been applied to various problems in nuclear physics, such as predicting atomic nuclear mass [24, 25], nuclear charge radii [26, 27], nuclear β-decay half-life [28], nuclear fission yields [29–31], spallation reactions [32–34], fragmentation reactions [35–37], and neutron nuclear reactions [38]. In this study, based on 475 experimental data points from 39 reaction systems induced by ^{6,7}Li, ^{9}Be, and ^{10}B, a BNN was constructed to evaluate the CF cross-sections of weakly bound nuclei for the first time. A systematic analysis of the suppression effect at energies above the Coulomb barrier was also conducted. The remainder of this paper is organized as follows. In Sect. 2, the main characteristics of the proposed BNN method are briefly described. Prediction results are presented in Sect. 3. Section 4 presents a summary.

2 Model descriptions

As a prominent machine learning technology, BNNs are highly effective for constructing novel models based on existing data. BNNs, which comprise a specific number of input units, hidden units of several layers, and output units, are capable of delivering high-quality predictions [39, 40]. This section presents a simple description of the BNN methodology. More detailed information can be found in [32, 35] and citations therein.

Bayesian learning sets the prior distribution of the model, $p(\omega)$, through the network parameter ω before observing any data, and updates the prior distribution to the posterior distribution $p(\omega|D)$ by observing the experimental data $D(x_i^n, y_j^n)$,

$$p(\omega|D) = \frac{p(D|\omega)p(\omega)}{p(D)} \propto p(D|\omega)p(\omega), \tag{1}$$

where the prior distribution is a Gaussian distribution with zero mean derived from the initial knowledge of the model. In the observed data $D(x_i^n, y_j^n)$, the outputs y_j^n correspond to the inputs x_i^n, where n,i,j are the number of data points, inputs, and outputs, respectively. The normalization function, $p(D)$, which ensures the posterior distribution in the effective probability density, is obtained through model assumptions with a prior integral,

$$p(D) = \int p(D|\omega)p(\omega)\mathrm{d}\omega. \tag{2}$$

The likelihood function, $p(D|w)$, is based on the Gaussian distribution of the objective function, χ^2, which fits the data using the least-squares method,

$$p(D|\omega) = \exp(-\chi^2/2), \tag{3}$$

$$\chi^2 = \sum_{i=1}^{N} \left[\frac{y_j^n - f_k^n(x_i^n;\omega)}{\Delta y_j^n} \right]^2. \tag{4}$$

Here Δy_j^n denotes the Gaussian noise corresponding to the n-th observation. A feedforward neural network is used for BNNs. This network typically includes a set of input variables, several hidden layers, and one or more output variables. A typical network function that connects outputs y_j^n to inputs x_i^n through a hidden layer is

$$f_k^n(x_i^n;\omega) = a_k + \sum_{j=1}^{N} b_{jk} \tanh\left(c_j + \sum_{i=1}^{I} d_{ij} x_i^n \right), \tag{5}$$

where N and I are the numbers of hidden units and inputs, respectively; (d_{ij}, c_j) and (b_{jk}, a_k) are the weights and biases of the hidden and output layers, respectively. The hidden unit values are obtained by a weighted summation of the input values acting on a hyperbolic tangent activation function (tanh), and the outputs $f_k^n(x_i^n;\omega)$ are obtained by a weighted summation of the hidden unit values and biases. The predicted distribution of the output y_j^{n+1} corresponding to the new input x_i^{n+1} is obtained from the posterior distribution as

$$p(y_j^{n+1}|x_i^{n+1}, D) = \int p(y_j^{n+1}|x_i^{n+1}, \omega)p(\omega|D)\mathrm{d}\omega. \tag{6}$$

To calculate the output data of the model, the Markov-chain Monte Carlo method is used to solve the high-dimensional integral

$$\langle y_j^{n+1} \rangle = \frac{1}{K} \sum_{k=1}^{K} f_k^n(x_i^{n+1};\omega_k), \tag{7}$$

where K denotes the number of iterations. The uncertainty of the predictions is obtained by $\Delta y_j = \sqrt{\langle y_j^2 \rangle - \langle y_j \rangle^2}$ because the model parameters are described using a probability distribution.

In this study, the dataset comprised the measured CF cross-sections in 39 reactions induced by ^{6,7}Li, ^{9}Be, and ^{10}B, giving rise to 475 data points, as detailed in Table 1 [41–68]. Within this dataset, the incident energy of the reactions ranges from $0.67V_b$ to $2.06V_b$, where V_b is the Coulomb barrier energy obtained from Akyüz-Winther nuclear potential and point-sphere Coulomb potential. The mass and charge of the target nuclei fall within the ranges of $64 \le A_t \le 209$ and $28 \le Z_t \le 83$, respectively. For model development, 380 data points (80% of all data) were randomly selected to form the training set, facilitating neural network learning and parameter optimization. The remaining 20% served as the test set to evaluate the prediction capabilities of the network. The input layer contains five parameters, $\{Z_p, A_p, Z_t, A_t, E_{cm}\}$, where Z_p and A_p represent the proton and mass numbers of the projectiles, respectively, and Z_t and A_t correspond to those of the targets. The parameter E_{cm} denotes the center-of-mass energy in MeV. The output parameter is the CF cross-section, denoted as σ_{exp}. Extensive efforts have been devoted to constructing hidden units by exploring single- and double-layer configurations. A double layer with 16 +16 neural units was ultimately verified as the most effective.

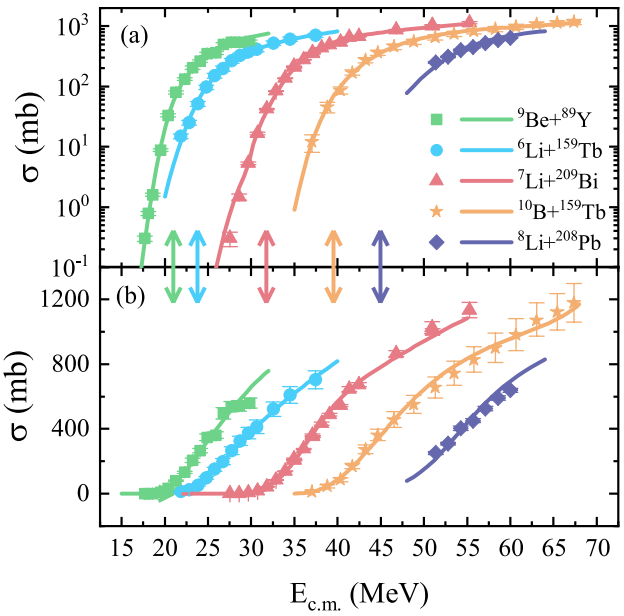

Fig. 1 (Color online) Comparison of the CF cross-sections obtained from the BNN model (solid lines) with experimental data (solid symbols) for ^{6}Li + ^{159}Tb, ^{7}Li + ^{209}Bi, ^{9}Be + ^{89}Y, ^{10}Be + ^{159}Tb, and ^{8}Li + ^{208}Pb systems. The logarithmic and linear scales are shown in (**a**) and (**b**), respectively. The arrows indicate the corresponding Coulomb barrier energies. Note that the energies for ^{7}Li + ^{209}Bi and ^{8}Li + ^{208}Pb are shifted by 1.1 and 1.6, respectively

3 Results and discussion

To verify the evaluation capacity of the BNN model, we performed a comparison between the predicted CF cross-sections and the experimental data, as depicted in Fig. 1. A logarithmic scale in Fig. 1a and a linear scale in Fig. 1b were adopted to compare the details of the cross-sections at sub-barrier and above-barrier energies, respectively. Taking the ^{6}Li + ^{159}Tb, ^{7}Li + ^{209}Bi, ^{9}Be + ^{89}Y, and ^{10}B + ^{159}Tb systems from the dataset as examples, the predicted results were in good agreement with the experimental CF cross-sections, both at sub-barrier and above-barrier energies. Furthermore, for the reaction system ^{8}Li + ^{208}Pb [69], which was not included in the dataset, the BNN model provided results consistent with the experimental data.

To further investigate the effects of the breakup channel on the fusion of weakly bound systems, a systematic analysis of the suppression factors of CF cross-sections at above-barrier energies is presented below. The suppression factors were obtained by fitting the CF cross-sections obtained from the BNN model or the experimental data using

$$F_{BNN} = \frac{\sigma_{BNN}}{\sigma_{BPM}} \quad \text{or} \quad F_{exp} = \frac{\sigma_{exp}}{\sigma_{BPM}}, \tag{8}$$

where σ_{BNN} and σ_{exp} are the predicted and measured cross-sections, respectively, and σ_{BPM} denotes the cross-sections calculated using a single-barrier potential model. The suppression factors calculated using the predicted CF cross-sections and experimental data are listed in the fourth and fifth columns of Table 1. Overall, the predictions of the BNN model represent the experimental suppression factors well. A detailed relationship between the suppression factor and mass number of the target nucleus A_t for ^{6}Li and ^{7}Li is shown in Fig. 2a, and the corresponding results for ^{9}Be and ^{10}B are shown in Fig. 2b. These target nuclei were mainly located in the relatively heavy-mass region, and no obvious dependence behavior was observed. In Fig. 2a, it is evident that the suppression factor of ^{7}Li is larger than that of ^{6}Li for the same mass target nuclei, which is attributed to the higher breakup threshold energies of ^{7}Li [22].

Next, we extended this BNN model to various mass regions of the target nucleus, including relatively light- and medium-mass targets. The CF cross-sections of ^{6,7}Li and ^{9}Be with the target nuclei along β stability line were predicted. The calculated suppression factors versus neutron, proton, and mass numbers of the targets are shown in Fig. 3. A surprising conclusion is that there is no suppression effect in the vicinity of $A_t = 110$ targets for ^{6,7}Li and ^{9}Be, and $A_t = 180$ targets for ^{6,7}Li. This was derived from the overall trend of the available experimental data; further experimental CF cross-sections are necessary to verify this conclusion.

In Fig. 3, the solid symbols denote the mean suppression factors derived from the targets with identical neutron (a), proton

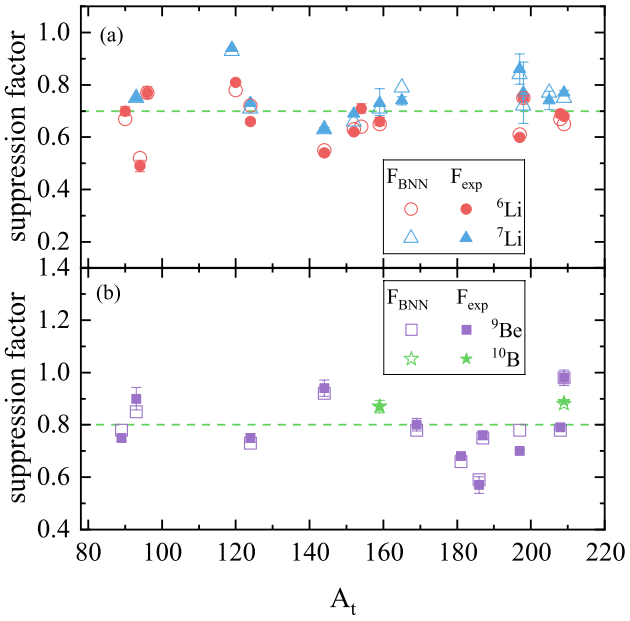

Fig. 2 (Color online) Suppression factors obtained from the BNN model (open symbols) and experimental data (full symbols) for fusion systems listed in Table 1. The reaction systems induced by ^{6}Li, ^{7}Li, ^{9}Be, and ^{10}B are represented by circles, triangles, squares, and stars, respectively. The horizontal dashed lines are the eye-guidance reference lines

(b), and mass (c) numbers. Dashed error bars indicate corresponding distribution ranges. Taking lead isotopes as an example, the predicted suppression factors of the BNN model for ^{7}Li + ^{204,206,207,208}Pb were 0.78, 0.77, 0.76, and 0.75, respectively. The mean suppression factor (0.765), upper limit of the error bar (0.78), and lower limit of the error bar (0.75) are located at $Z_t = 82$ in Fig. 3(b). Consequently, the range of error bars indicates the dependence of the suppression effect on the isotone, isotope, and isobar target nuclei. The small error bars of ^{6}Li and ^{7}Li suggest weak dependence, whereas the suppression factors of ^{9}Be exhibit strong dependence. Owing to this sensitivity to the number of nucleons in the target nucleus, there is a pronounced fluctuation in various target nuclei for ^{9}Be. This makes it difficult to identify a systematic trend for ^{9}Be.

For ^{6}Li and ^{7}Li, the consistent behavior of the mean suppression factor suggests that they possess a similar breakup mechanism, and the minimum values of the suppression factor occur near the target nuclei with a neutron-closed shell. Within the relatively light-mass target region ($60 \le A_t \le 90$), the suppression factors for ^{6}Li and ^{7}Li remain around 0.8 and 0.9, respectively, which is significantly less suppression than that observed for heavy targets ($120 \le A_t \le 160$). Moreover, the systematic behaviors in different mass target regions are markedly distinct. For light-mass targets, the suppression factor varies with the target nucleus mass number, initially increasing and then decreasing. By contrast, in the heavy-mass target region, the suppression factor initially decreases and then increases. This indicates that there is a competitive process in the breakup mechanism and that the primary breakup channel may differ across various mass target regions. Owing to the limitations of machine learning and the complexity of the breakup processes, it is challenging to provide a specific physical mechanism. More experimental and theoretical research is required to verify these conclusions and provide more explanations for the underlying breakup mechanism.

4 Summary

In this study, we investigated the complete fusion reactions of weakly bound nuclei using machine learning methods. A BNN was constructed based on 475 existing experimental

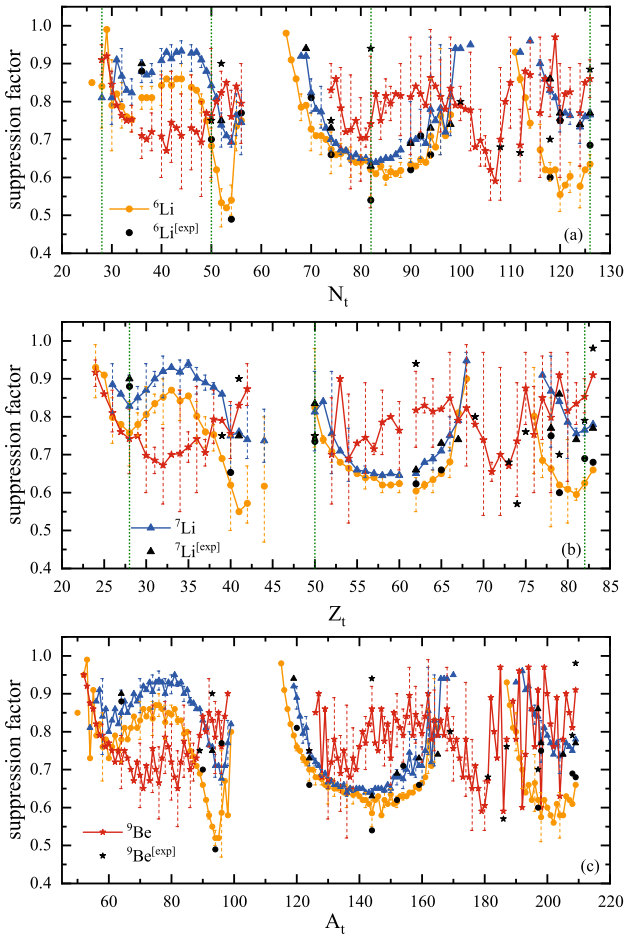

Fig. 3 (Color online) Relationship between the suppression factors and the neutron (**a**), proton (**b**), and mass (**c**) numbers of the target nuclei for projectile nuclei ^{6}Li (orange circles), ^{7}Li (blue triangles), and ^{9}Be (red stars). The symbols denote the mean suppression factor whereas the dashed error bars indicate the distribution range. The black symbols denote the corresponding experimental suppression factors. The magic numbers are located by the vertical dotted lines. The solid lines guide the eye. (See the text for more details.)

Table 1 The 39 fusion systems induced by weakly bound projectile nuclei ^{6,7}Li, ^{9}Be, and ^{10}B

Reaction	E_{cm}/V_B	N_{exp}	F_{BNN}	F_{exp}	Ref	Reaction	E_{cm}/V_B	N_{exp}	F_{BNN}	F_{exp}	Ref
^{6}Li+^{64}Ni	0.85−2.06	15	0.87	0.88	[41]	^{7}Li+^{159}Tb	1.07−1.66	5	0.71	0.73	[57]
^{6}Li+^{90}Zr	0.82−1.65	8	0.67	0.7	[17]	^{7}Li+^{165}Ho	0.86−1.69	10	0.79	0.74	[15]
^{6}Li+^{94}Zr	0.89−1.68	5	0.52	0.49	[7]	^{7}Li+^{197}Au	0.81−1.50	8	0.84	0.86	[50]
^{6}Li+^{96}Zr	0.90−1.58	7	0.77	0.77	[42]	^{7}Li+^{198}Pt	0.79−1.52	6	0.72	0.77	[58]
^{6}Li+^{120}Sn	0.74−1.32	13	0.78	0.81	[43, 44]	^{7}Li+^{205}Tl	0.82−1.31	10	0.77	0.74	[59]
^{6}Li+^{124}Sn	0.83−1.70	15	0.72	0.66	[45]	^{7}Li+^{209}Bi	0.83−1.67	21	0.75	0.77	[53]
^{6}Li+^{144}Sm	0.79−1.58	11	0.55	0.54	[46]	^{9}Be+^{89}Y	0.83−1.39	15	0.78	0.75	[60]
^{6}Li+^{152}Sm	0.80−1.60	20	0.63	0.62	[47]	^{9}Be+^{93}Nb	0.85−1.45	7	0.85	0.90	[61]
^{6}Li+^{154}Sm	1.04−1.45	6	0.64	0.71	[48]	^{9}Be+^{124}Sn	0.90−1.33	13	0.73	0.75	[62]
^{6}Li+^{159}Tb	0.87−1.50	13	0.65	0.66	[49]	^{9}Be+^{144}Sm	0.89−1.31	10	0.92	0.94	[63]
^{6}Li+^{197}Au	0.84−1.35	16	0.61	0.60	[50]	^{9}Be+^{169}Tm	0.93−1.33	12	0.78	0.80	[64]
^{6}Li+^{198}Pt	0.67−1.14	10	0.75	0.75	[51]	^{9}Be+^{181}Ta	0.94−1.34	13	0.66	0.68	[65]
^{6}Li+^{208}Pb	0.92−1.28	20	0.67	0.69	[52]	^{9}Be+^{186}W	1.08−1.40	4	0.59	0.57	[66]
^{6}Li+^{209}Bi	0.83−1.53	14	0.65	0.68	[53]	^{9}Be+^{187}Re	0.93−1.28	12	0.75	0.76	[64]
^{7}Li+^{64}Ni	0.87−2.06	16	0.90	0.90	[54]	^{9}Be+^{197}Au	0.83−1.17	12	0.78	0.70	[67]
^{7}Li+^{93}Nb	1.29−1.63	4	0.75	0.75	[55]	^{9}Be+^{208}Pb	0.88−1.24	16	0.78	0.79	[53]
^{7}Li+^{119}Sn	0.72−1.30	15	0.93	0.94	[43, 44]	^{9}Be+^{209}Bi	0.88−1.21	19	0.98	0.98	[52]
^{7}Li+^{124}Sn	0.79−1.86	23	0.71	0.73	[56]	^{10}B+^{159}Tb	0.91−1.66	16	0.87	0.87	[57]
^{7}Li+^{144}Sm	0.88−1.59	14	0.63	0.63	[18]	^{10}B+^{209}Bi	1.06−1.44	5	0.88	0.89	[68]
^{7}Li+^{152}Sm	0.81−1.61	16	0.66	0.69	[18]						

The symbols E_{cm} and V_b denote the center-of-mass energy and Coulomb barrier energy, respectively. N_{exp} represents the numbers of experimental CF cross-section. F_{BNN} and F_{exp} denote the suppression factors calculated by Ep. (8). The last column provides the corresponding reference where the measured cross-sections were taken from

complete fusion data points induced by ^{6,7}Li, ^{9}Be, and ^{10}B. This model characterizes five input parameters (projectile and target information, and colliding energy), double hidden layers (16 + 16 neural units), and one output parameter (CF cross-section). The CF cross-sections predicted by this model exhibited excellent agreement with the experimental data, demonstrating the high-quality predictive capabilities of the model.

The suppression factors, defined as the ratio of the CF cross-sections predicted by BNN model to those calculated by a single-barrier penetration model at above-barrier energies, were systematically analyzed for weakly bound projectiles ^{6,7}Li and ^{9}Be with the target nuclei along the β stability line. The dependence behavior of the suppression effect was predicted across various mass target regions, particularly for relatively light-mass targets. For ^{9}Be, the suppression factors exhibited a marked sensitivity to the target nucleus, and no apparent systematic behavior was observed in either the heavy- or light-mass target regions. For ^{6}Li and ^{7}Li, the BNN model predicted less suppression in relatively light-mass targets compared to that observed for heavy-mass targets. Furthermore, the dependence in the light-mass target region was exactly opposite to that in the heavy-mass target region. These conclusions require further experimental and theoretical validation, as well as mechanistic explanations.

Author Contributions All authors contributed to the conception of this study. Coding was performed by Rong-Xing He. Kai-Xuan Cheng was responsible for code review, analysis, and result checking. The project was leaded and supervised by Kai-Xuan Cheng and Chun-Wang Ma. The first draft of the manuscript was written by Kai-Xuan Cheng and modified by Rong-Xing He, Chun-Yuan Qiao, and Chun-Wang Ma. All authors read and approved the final versions of the manuscript.

Data Availability The data that support the findings of this study are openly available in Science Data Bank at https://cstr.cn/31253.11.sciencedb.26766 and http://doi.org/ 10.57760/sciencedb.26766.

Declarations

Conflict of interest Chun-Wang Ma is an editorial board member for Nuclear Science and Techniques and was not involved in the editorial review, or the decision to publish this article. All authors declare that there are no Conflict of interest.

References

1. L.F. Canto, P.R.S. Gomes, R. Donangelo et al., Recent developments in fusion and direct reactions with weakly bound nuclei. Phys. Rept. **596**, 1 (2015). https://doi.org/10.1016/j.physrep.2015.08.001

2. Y.L. Ye, X.F. Yang, H. Sakurai et al., Physics of exotic nuclei. Nat. Rev. Phys. **7**, 21–37 (2024). https://doi.org/10.1038/s42254-024-00782-5
3. L.F. Canto, V. Guimaraes, J. Lubian et al., The total reaction cross section of heavy-ion reactions induced by stable and unstable exotic beams: the low-energy regime. Eur. Phys. J. A **56**, 281 (2020). https://doi.org/10.1140/epja/s10050-020-00277-8
4. K. Hagino, K. Ogata, A. Moro, Coupled-channels calculations for nuclear reactions: From exotic nuclei to superheavy elements. Prog. Part. Nucl. Phys. **125**, 103951 (2022). https://doi.org/10.1016/j.ppnp.2022.103951
5. L. Yang, C.J. Lin, H. Yamaguchi et al., Breakup of the proton halo nucleus ^{8}B near barrier energies. Nat. Commun. **13**, 7193 (2022). https://doi.org/10.1038/s41467-022-34767-8
6. G.L. Zhang, Z.W. Jiao, G.X. Zhang et al., Further investigation on the fusion of ^{6}Li with ^{209}Bi target at near-barrier energies. Chin. Phys. C **48**, 074001 (2024). https://doi.org/10.1088/1674-1137/ad4264
7. X.D. Su, G.X. Zhang, S.P. Hu et al., Fusion and one-neutron stripping process for ^{6}Li + ^{94}Zr system around the Coulomb Barrier. Chin. Phys. C **48**, 094001 (2024). https://doi.org/10.1088/1674-1137/ad50b9
8. Y.D. Fang, P.R.S. Gomes, J. Lubian et al., Complete and imcomplete fusion of ^{9}Be + ^{169}Tm, ^{187}Re at near barrier energies. Phys. Rev. C **91**, 014608 (2015). https://doi.org/10.1103/PhysRevC.91.014608
9. A.D. Torres, D.J. Hinde, J.A. Tostevin et al., Relating breakup and incomplete fusion of weakly bound nuclei through a classical trajectory model with stochastic breakup. Phys. Rev. Lett. **98**, 152701 (2007). https://doi.org/10.1103/PhysRevLett.98.152701
10. L. Jin, A.M. Moro, Puzzle of complete fusion suppression in weakly bound nuclei: A trojan horse effect? Phys. Rev. Lett. **122**, 042503 (2019). https://doi.org/10.1103/PhysRevLett.122.042503
11. L. Jin, A.M. Moro, Unraveling the reaction mechanisms leading to partial fusion of weakly bound nuclei. Phys. Rev. Lett. **123**, 232501 (2019). https://doi.org/10.1103/PhysRevLett.123.232501
12. M. Dasgupta, L.R. Gasques, D.H. Luong et al., Reaction dynamics of weakly bound nuclei at near-barrier energies. Nucl. Phys. A **834**, 147c–150c (2010). https://doi.org/10.1016/j.nuclphysa.2009.12.025
13. P.R.S. Gomes, D.R. Otomar, T. Correa et al., Complete fusion enhancement and suppression of weakly bound nuclei at near barrier energies. J. Phys. G: Nucl. Part. Phys. **39**, 115103 (2012). https://doi.org/10.1088/0954-3899/39/11/115103
14. V.V. Sargsyan, G.G. Adamian, N.V. Antonenko et al., Search for a systematic behavior of the breakup probability in reactions with weakly bound projectiles at energies around the Coulomb barrier. Phys. Rev. C **86**, 054610 (2012). https://doi.org/10.1103/PhysRevC.86.054610
15. V. Tripathi, A. Navin, K. Mahata et al., Angular momentum and cross sections for fusion with weakly bound nuclei: Breakup, a coherent effect. Phys. Rev. Lett. **88**, 172701 (2002). https://doi.org/10.1103/PhysRevLett.88.172701
16. V. Tripathi, A. Navin, V. Nanal et al., Experimental signatures for distinguishing breakup fusion and transfer in ^{7}Li +^{165} Ho. Phys. Rev. C **72**, 017601 (2005). https://doi.org/10.1103/PhysRevC.72.017601
17. H. Kumawat, V. Jha, V.V. Parkar et al., Fusion reaction studies for the ^{6}Li + ^{90}Zr system at near-barrier energies. Phys. Rev. C **86**, 024607 (2012). https://doi.org/10.1103/PhysRevC.86.024607
18. P.K. Rath, S. Santra, N.L. Singh et al., Complete fusion in ^{7}Li + ^{144,152}Sm reactions. Phys. Rev. C **88**, 044617 (2013). https://doi.org/10.1103/PhysRevC.88.044617
19. K.X. Cheng, J. Pu, Y.T. Wang et al., Non-frozen process of heavy-ion fusion reactions at deep sub-barrier energies. Nucl. Sci. Tech. **33**, 132 (2022). https://doi.org/10.1007/s41365-022-01114-x
20. S.P. Hu, G.L. Zhang, J.C. Yang et al., Small suppression of the complete fusion of the ^{6}Li + ^{96}Zr system at near-barrier energies. Phys. Rev. C **91**, 044619 (2015). https://doi.org/10.1103/PhysRevC.91.044619
21. K.J. Cook, E.C. Simpson, L.T. Bezzina et al., Origins of imcomplete fusion products and the suppression of complete fusion in reactions of ^{7}Li. Phys. Rev. Lett. **122**, 102501 (2019). https://doi.org/10.1103/PhysRevLett.122.102501
22. B. Wang, W.J. Zhao, P.R.S. Gomes et al., Systematic study of breakup effects on complete fusion at energies above the Coulomb barrier. Phys. Rev. C **90**, 034612 (2014). https://doi.org/10.1103/PhysRevC.90.034612
23. P.R.S. Gomes, R. Linares, J. Lubian et al., Search for systematic behavior of incomplete-fusion probability and complete-fusion suppression induced by ^{9}Be on different targets. Phys. Rev. C **84**, 014615 (2011). https://doi.org/10.1103/PhysRevC.84.014615
24. Z.M. Niu, H.Z. Liang, Nuclear mass predictions based on Bayesian neural network approach with pairing and shell effects. Phys. Lett. B **778**, 48 (2018). https://doi.org/10.1016/j.physletb.2018.01.002
25. Z.M. Niu, H.Z. Liang, Nuclear mass predictions with machine learning reaching the accuracy required by r-process studies. Phys. Rev. C **106**, L021303 (2022). https://doi.org/10.1103/PhysRevC.106.L021303
26. Y.F. Ma, C. Su, J. Liu et al., Predictions of nuclear charge radii and physical interpretations based on the Naive Bayesian probability classifier. Phys. Rev. C **101**, 014304 (2020). https://doi.org/10.1103/PhysRevC.101.014304
27. X.X. Dong, R. An, J.X. Lu et al., Nuclear charge radii in Bayesian neural networks revisited. Phys. Lett. B **838**, 137726 (2023). https://doi.org/10.1016/j.physletb.2023.137726
28. Z.M. Niu, H.Z. Liang, B.H. Sun et al., Predictions of nuclear β -decay half-lives with machine learning and their impact on r -process nucleosynthesis. Phys. Rev. C **99**, 064307 (2019). https://doi.org/10.1103/PhysRevC.99.064307
29. C.Y. Qiao, J.C. Pei, Z.A. Wang et al., Bayesian evaluation of charge yields of fission fragments of ^{239}U. Phys. Rev. C **103**, 034621 (2021). https://doi.org/10.1103/PhysRevC.103.034621
30. Z.A. Wang, J.C. Pei, Y. Liu et al., Bayesian evaluation of incomplete fission yields. Phys. Rev. Lett. **123**, 122501 (2019). https://doi.org/10.1103/PhysRevLett.123.122501
31. Z.A. Wang, J.C. Pei, Optimizing multilayer Bayesian neural networks for evaluation of fission yields. Phys. Rev. C **104**, 064608 (2021). https://doi.org/10.1103/PhysRevC.104.064608
32. C.W. Ma, D. Peng, H.L. Wei, Isotopic cross-sections in proton induced spallation reactions based on the Bayesian neural network method. Chin. Phys. C **44**, 014104 (2020). https://doi.org/10.1088/1674-1137/44/1/014104
33. C.W. Ma, D. Peng, H.L. Wei et al., A Bayesian-Neural-Network prediction for fragment production in proton induced spallation reaction. Chin. Phys. C **44**, 124107 (2020). https://doi.org/10.1088/1674-1137/abb657
34. D. Peng, H.L. Wei, X.X. Chen et al., Bayesian evaluation of residual production cross sections in proton-induced nuclear spallation reactions. J. Phys. G: Nucl. Part. Phys. **49**, 085102 (2022). https://doi.org/10.1088/1361-6471/ac7069
35. C.W. Ma, X.B. Wei, X.X. Chen et al., Precise machine learning models for fragment production in projectile fragmentation reactions using Bayesian neural networks. Chin. Phys. C **46**, 074104 (2022). https://doi.org/10.1088/1674-1137/ac5efb
36. C.W. Ma, X.X. Chen, X.B. Wei et al., Systematic behavior of fragments in Bayesian neural network models for projectile

fragmentation reactions. Phys. Rev. C **108**, 044606 (2023). https://doi.org/10.1103/PhysRevC.108.044606
37. X.B. Wei, H.L. Wei, Y.T. Wang et al., Multiple-models predictions for drip line nuclides in projectile fragmentation of ^{40,48}Ca, ^{58,64}Ni, and ^{78,86}Kr at 140MeV/u. Nucl. Sci. Tech. **33**, 155 (2023). https://doi.org/10.1007/s41365-022-01137-4
38. W.F. Li, L.L. Liu, Z.M. Niu et al., Predictions for (n, 2n) reaction cross section based on a Bayesian neural network approach. Phys. Rev. C **109**, 044616 (2024). https://doi.org/10.1103/PhysRevC.109.044616
39. A. Boehnlein, M. Diefenthaler, N. Sato et al., Colloquium: Machine learning in nuclear physics. Rev. Mod. Phys. **94**, 031003 (2022). https://doi.org/10.1103/RevModPhys.94.031003
40. W.B. He, Q.F. Li, Y.G. Ma et al., Machine learning in nuclear physics at low and intermediate energies. Science China: Phys Mech Astron **66**, 282001 (2023). https://doi.org/10.1007/s11433-023-2116-0
41. M.M. Shaikh, S. Roy, S. Rajbanshi et al., Investigation of ^{6}Li + ^{64}Ni fusion at near-barrier energies. Phys. Rev. C **90**, 024615 (2014). https://doi.org/10.1103/PhysRevC.90.024615
42. S.P. Hu, G.L. Zhang, J.C. Yang et al., Small suppression of the complete fusion of the ^{6}Li + ^{96}Zr system at near-barrier energies. Phys. Rev. C **91**, 044619 (2015). https://doi.org/10.1103/PhysRevC.91.044619
43. N. Grover, I. Sharma, M.S. Gautam et al., Fusion and decay dynamics of ^{6}Li + ^{120}Sn and ^{7}Li + ^{119}Sn reactions across the Coulomb barrier. Phys. Rev. C **108**, 064607 (2023). https://doi.org/10.1103/PhysRevC.108.064607
44. M. Fisichella, A.C. Shotter, P. Figuera et al., Breakup and n -transfer effects on the fusion reactions ^{6,7}Li + ^{120,119}Sn around the Coulomb barrier. Phys. Rev. C **95**, 034617 (2017). https://doi.org/10.1103/PhysRevC.95.034617
45. V.V. Parkar, S.K. Pandit, A. Shrivastava et al., Fusion reaction studies for the ^{6}Li + ^{124}Sn system at near-barrier energies. Phys. Rev. C **98**, 014601 (2018). https://doi.org/10.1103/PhysRevC.98.014601
46. P.K. Rath, S. Santra, N.L. Singh et al., Suppression of complete fusion in the ^{6}Li + ^{144}Sm reaction. Phys. Rev. C **79**, 051601 (2009). https://doi.org/10.1103/PhysRevC.79.051601
47. P.K. Rath, S. Santra, N.L. Singh et al., Fusion of ^{6}Li with ^{152} Sm: Role of projectile breakup versus target deformation. Nucl. Phys. A **874**, 14 (2012). https://doi.org/10.1016/j.nuclphysa.2011.10.004
48. C.L. Guo, G.L. Zhang, S.P. Hu et al., Coupling effects on the fusion of ^{6}Li + ^{154}Sm at energies slightly above the Coulomb barrier. Phys. Rev. C **92**, 014615 (2015). https://doi.org/10.1103/PhysRevC.92.014615
49. M.K. Pradhan, A. Mukherjee, P. Basu et al., Fusion of ^{6}Li with ^{159}Tb at near barrier energies. Phys. Rev. C **83**, 064606 (2011). https://doi.org/10.1103/PhysRevC.83.064606
50. C. S. Palshetkar1, S. Thakur, V. Nanal et al., Fusion and quasielastic scattering in the ^{6,7}Li + ^{197}Au systems. Phys. Rev. C **89**, 024607 (2014). [Erratum: Phys.Rev.C **100**, 039902 (2019)] http://dx.doi.org/10.1103/PhysRevC.89.024607
51. A. Shrivastava, A. Navin, A. Lemasson et al., Exploring fusion at extreme sub-barrier energies with weakly bound nuclei. Phys. Rev. Lett. **103**, 232702 (2009). https://doi.org/10.1103/PhysRevLett.103.232702
52. Z.H. Liu, C. Signorini, M. Mazzocco et al., Partial fusion of a weakly bound projectile with heavy target at energies above the Coulomb barrier. Eur. Phys. J. A **26**, 73 (2005). https://doi.org/10.1140/epja/i2004-10305-4
53. M. Dasgupta, P.R.S. Gomes, D.J. Hinde et al., Effect of breakup on the fusion of ^{6}Li, ^{7}Li, and ^{9}Be with heavy nuclei. Phys. Rev. C **70**, 024606 (2004). https://doi.org/10.1103/PhysRevC.70.024606
54. M.M. Shaikh, S. Roy, S. Rajbanshi et al., Probing the fusion of ^{7}Li with ^{64}Ni at near-barrier energies. Phys. Rev. C **93**, 044616 (2016). https://doi.org/10.1103/PhysRevC.93.044616
55. S.K. Pandit, A. Shrivastava, K. Mahata et al., Investigation of large α production in reactions involving weakly bound ^{7}Li. Phys. Rev. C **96**, 044616 (2017). https://doi.org/10.1103/PhysRevC.96.044616
56. V.V. Parkar, S.K. Sharma, R. Palit et al., Investigation of complete and incomplete fusion in the ^{7}Li + ^{124}Sn reaction near Coulomb barrier energies. Phys. Rev. C **97**, 014607 (2018). https://doi.org/10.1103/PhysRevC.97.014607
57. A. Mukherjee, S. Roy, M.K. Pradhan et al., Influence of projectile alpha- breakup threshold on complete fusion. Phys. Lett. B **636**, 91 (2006). https://doi.org/10.1016/j.physletb.2006.03.051
58. A. Shrivastava, A. Navin, A.D. Torres et al., Role of the cluster structure of ^{7}Li in the dynamics of fragment capture. Phys. Lett. B **718**, 931 (2013). https://doi.org/10.1016/j.physletb.2012.11.064
59. V.V. Parkar, M. Prasanna, R. Ruchi et al., Fusion of ^{7}Li with ^{205}Tl at near-barrier energies. Phys. Rev. C **109**, 014610 (2024). https://doi.org/10.1103/PhysRevC.109.014610
60. C.S. Palshetkar, S. Santra, A. Chatterjee et al., Fusion of the weakly bound projectile ^{9}Be with ^{89}Y. Phys. Rev. C **82**, 044608 (2010). https://doi.org/10.1103/PhysRevC.82.044608
61. H. Sharma, M. Maiti, M. Sagwa et al., Study of ^{9}Be fusion in ^{93}Nb near the Coulomb barrier. Eur. Phys. J. A **60**, 64 (2024). https://doi.org/10.1140/epja/s10050-024-01296-5
62. V.V. Parkar, R. Palit, S.K. Sharma et al., Fusion cross sections for the ^{9}Be + ^{124}Sn reaction at energies near the Coulomb barrier. Phys. Rev. C **82**, 054601 (2010). https://doi.org/10.1103/PhysRevC.82.054601
63. P.R.S. Gomesa, J. Lubiana, B. Paes et al., Near-barrier fusion, breakup and scattering for the ^{9}Be + ^{144}Sm system. Nucl. Phys. A **828**, 233 (2009). https://doi.org/10.1016/j.nuclphysa.2009.07.008
64. Y.D. Fang, P.R.S. Gomes, J. Lubian et al., Complete and incomplete fusion of ^{9}Be + ^{169}Tm,^{187}Re at near-barrier energies. Phys. Rev. C **91**, 014608 (2015). https://doi.org/10.1103/PhysRevC.91.014608
65. N.T. Zhang, Y.D. Fang, P.R.S. Gomes et al., Complete and incomplete fusion in the ^{9}Be + ^{181}Ta reaction. Phys. Rev. C **90**, 024621 (2014). https://doi.org/10.1103/PhysRevC.90.024621
66. Y.D. Fang, P.R.S. Gomes, J. Lubian et al., Fusion and one-neutron stripping reactions in the ^{9}Be +^{186}W system above the Coulomb barrier. Phys. Rev. C **87**, 024604 (2013). https://doi.org/10.1103/PhysRevC.87.024604
67. M. Kaushik, G. Gupta, S. Thakur et al., Fusion of the Borromean nucleus ^{9}Be with a ^{197}Au target at near-barrier energies. Phys. Rev. C **101**, 034611 (2020). https://doi.org/10.1103/PhysRevC.101.034611
68. L.R. Gasques, D.J. Hinde, M. Dasgupta et al., Suppression of complete fusion due to breakup in the reactions ^{10,11}B + ^{209}Bi. Phys. Rev. C **79**, 034605 (2009). https://doi.org/10.1103/PhysRevC.79.034605
69. E.F. Aguilera, E.M. Quiroz, P. Rosales et al., Hindrance of complete fusion in the ^{8}Li + ^{208}Pb system at above-barrier energies. Phys. Rev. C **80**, 044605 (2009). https://doi.org/10.1103/PhysRevC.80.044605